ASPECTS OF PHASE SPACE DYNAMICS IN SPIRAL INFLECTORS

R.J. Balden, W. Kleeven, L.S. Milinkovic, B.F. Milton, and J.B. Pearson,
TRIUMF, 4004 Wesbrook Mall, Vancouver, B.C. V6T 2A3

ABSTRACT

The equations of motion for paraxial rays in a pseudo cylindrical electrostatic inflector with tilt have been known for some time. Unfortunately the origin of the various components of the electric field expansion are more poorly documented. In this paper we present a physical interpretation for each element of the electric field and then discuss how the resulting field expansion might be implemented in a FORTRAN program that tracks particles in a general magnetic field. Results from such a program are then used together with an acceptance calculation program, to study the question of inflector acceptance as a function of several inflector parameters.

1. INTRODUCTION

Spiral inflectors have been used for axial injection into cyclotrons for some time.[1] The equations of motion are well known for the case of untilted,[2,3] and tilted[4] inflectors. The equations are derived from an expansion of the electric field about the central ray. This was first done for the general case of tilted inflectors by Root.[4] We begin by reviewing the terms in this expansion, with the aim of clarifying their origin, and giving a physical interpretation of each.

We then describe a general inflector tracking code CASINO[5] (**Ca**lculation of **S**piral **In**flector **O**rbits). It uses a general magnetic field, and an analytic or numerically calculated electric field. CASINO therefore combines the features of Root's AXORB[3] and ORBIT[3] programs in an updated FORTRAN code. Additionally, it incorporates an analytic model for the fringe field of the inflector, which becomes important for short inflectors. Paraxial rays can be specified in special inflector optical coordinate systems.

We then describe a program to calculate the acceptance of an inflector, using data output from CASINO. We have used these two programs together to study the reduction of the acceptance of inflectors, (discussed by Belmont[1] and Marti[6]), as a function of the inflector parameters.

2. ELECTRIC FIELD EXPANSION

In the case of a homogeneous magnetic field it is well known[2] that analytic expressions can be found for the central ray trajectory, $(x(b), y(b), z(b)$, with injection along the z axis), in terms of the angle in the bend plane (b). In addition, one needs the usual parameters of the inflector,[2]

$$K = \frac{A}{2R}\,, \tag{1}$$

$$k' = \frac{\tan\theta}{\sin b}\,, \tag{2}$$

where A is the electric radius and R is the magnetic radius. If the inflector is tilted (slanted), then the tilt parameter (k') may be used to adust the centring of the beam at the inflector exit. In this case the electrodes are rotated by an angle (θ) as one proceeds through the inflector. In order to retain a closed form solution the electrodes must be tapered in such a way as to keep the component of the electric field in the bend plane constant as the electrodes rotate.

To study the optics of paraxial rays, it is conventional to use two optical coordinate systems,[3] both of which move along with the central ray. The first system has basis vectors $\hat{u}, \hat{h}, \hat{v}$; where $\hat{v}$ points along the beam direction, $\hat{h}$ is in the horizontal (x, y) plane, and $\hat{u} = \hat{h} \times \hat{v}$. The second, so called rotated, coordinate system is defined by rotating the first system, through an angle (θ) about the vector $\hat{v}$, and has basis vectors $\hat{u}_r, \hat{h}_r, \hat{v}$. The electric force on the central ray always points in the $\hat{u}_r$ direction.

In both systems, the coordinates of a paraxial ray may be defined in terms of the displacement from the central ray $(\vec{dr})$, projected onto the optical coordinate system. In the rotated system for example, $\vec{dr} = u_r\hat{u}_r + h_r\hat{h}_r + v\hat{v}$.

The behaviour of a paraxial ray may be studied using an electric field which is expanded linearly about the electric field along the central ray $(\vec{E}_{cr} = \vec{E}(b, 0, 0))$. This expansion has been carried out by Root[4] for the general

case of an inflector with tilt and is based on the expansion

$$\Delta\vec{E}(v,h_r,u_r) = \vec{E}(b,h_r,u_r) - \vec{E}(b,0,0) + \frac{v}{A}\left.\frac{\partial\vec{E}}{\partial b}\right|_{h_r,u_r=0} . \tag{3}$$

The central ray is confined to lie on an equipotential surface, and therefore $\vec{E}(b,0,0) = -|E_{cr}|\hat{n}$, where $\hat{n}$ is the unit vector normal to the equipotential surface and the minus sign is for negative ions. As one moves away from the central ray in the $\hat{u}_r$ or $\hat{h}_r$ direction, there is a variation in both $|E|$ and $\hat{n}$. The normal vector may be expressed as,

$$\hat{n}(u_r,h_r) = \hat{u}_r - h_r\frac{\hat{h}_r}{ds}\times\hat{h}_r + \frac{u_r}{E_{cr}}\frac{\partial E_{cr}}{\partial s}\hat{v} , \tag{4}$$

where $s = bR$ is the arc length along the trajectory. A displacement in the $\hat{h}_r$ direction produces a rotation of $\hat{n}$ about the $\hat{h}_r$ vector, which may be derived using results from the differential geometry of ruled surfaces as outlined by Root.[3,4] Retaining terms to first order, this yields the second term in eq. (4). This effect is similar to the steepening of a spiral staircase as one moves toward the centre. In addition $\hat{n}$ rotates when one moves in the $\hat{u}_r$ direction, due to the taper of the electrodes.[5] This term (the third in eq. (4)) is included in Root's final expansion for the electric field, but his derivation does not include it explicitly.

The magnitude of the electric field must also change as one moves along the $\hat{u}_r$ direction because the curvature of the equipotential surfaces is increasing. Assuming that the magnitude of the electric field is similar to that in a cylindrical capacitor then we can use the well known electrostatics result,

$$E(b,u_r,0) = E_{cr}\frac{r_0}{r_0-u_r} \approx E_{cr}\left(1+\frac{u_r}{r_0}\right) , \tag{5}$$

where r_0 is the instantaneous radius of curvature.

Finally, the last term in eq. (3), involving the variation in (b) may be evaluated using $\frac{\partial}{\partial s} = \frac{1}{A}\frac{\partial}{\partial b}$, and the chain rule,

$$\left.\frac{\partial\vec{E}}{\partial b}\right|_{h_r,u_r=0} = \frac{\partial|E|}{\partial b}\hat{u}_r + |E|\frac{\partial\hat{u}_r}{\partial b} , \tag{6}$$

where Root's expressions for $\hat{u}_r$ as a function of time may be used, as outlined elsewhere.[4,5,7]

The substitution of eqs. (4)-(6) into equation (3), while retaining only first order terms is straight forward, but involved. The result, as given by Root[4] is,

$$\begin{aligned}\Delta\vec{E} = \frac{E_0}{A}\Bigg[&\left(\frac{k'^2\sin(b)\cos(b)}{\sqrt{1+k'^2\sin^2(b)}}v + [1+2Kk'\sin^2(b)]u_r\right)\hat{u}_r \\ &+ v\left(2K\cos(b)\sqrt{1+k'^2\sin^2(b)} + \frac{k'\cos(b)}{\sqrt{1+k'^2\sin^2(b)}}\right)\hat{h}_r \\ &+ \left(\frac{k'^2\sin(b)\cos(b)}{\sqrt{1+k'^2\sin^2(b)}}u_r - [1+2Kk'\sin^2(b)]v\right. \\ &\left.+ [2K\cos(b)\sqrt{1+k'^2\sin^2(b)} + \frac{k'\cos(b)}{\sqrt{1+k'^2\sin^2(b)}}]h_r\right)\hat{v}\Bigg] ,\end{aligned}$$

and the intermediate steps have been shown in more detail elsewhere.[5,7] In brief then, the terms in the above equation can be seen to arise from the following causes. The rotation of $\hat{n}$ due to displacements in $\hat{h}_r$ (the effective steepening of the spiral), produces the seventh and eighth terms. The rotation of $\hat{n}$ due to displacements in $\hat{u}_r$ (the term arising from the taper of the electrodes) produces the fifth term. The cylindrical capacitor scaling of $|E|$ is responsible for the second term. The remaining terms, all proportional to v, arise from the $\frac{\partial}{\partial b}$ terms in eq. (3). It can be seen that they serve to force $\Delta\vec{E}$ to obey Maxwell's equations. It should be noted that the first and fifth terms need not be present if the electrodes are untapered.

3. CALCULATION OF INFLECTOR ORBITS

In the more general case, when the magnetic field is non-homogeneous, when the tilt is arbitrarily defined, or when the electrodes are untapered, a closed form solution for the central ray trajectory is no longer possible. The calculation of the electric field is then somewhat more complicated, and we will discuss this in the context of a program which tracks particles in the general case.

The program CASINO is a fourth order Runge-Kutta tracking code. It tracks particles in a magnetic field which may be specified as i) homogeneous, ii) $B_z(z)$ (the field along the magnet axis, or iii) $B_z(z,r)$ (as provided by POISSON for example). The electric field may be computed in an analytic manner, or computed from an electric potential map (as provided for example by RELAX3D[8]). Our RELAX3D calculations are done with the aid of the subroutine INFLECTOR,[9] which prescribes the inflector electrode locations in RELAX3D. This subroutine takes its input from a file generated by CASINO, so that a RELAX3D inflector can be generated around an analytic central ray.

The approach to the expansion of the analytic electric field is, in many ways, similar to the case of the homogeneous magnetic field, but with time as the independent variable. The central ray is still assumed to run on an equipotential. During the calculation of the central ray, the coordinates of the central ray, the optical coordinates, and the magnitude of the electric field at the end of each integration step are stored. Following this the paraxial rays are run. The expansion of the electric field for the paraxial ray is done with respect to the point on the central ray produced by a perpendicular projection of the paraxial particle onto the central ray. The values stored along the central ray for the optical coordinates, and the derivatives $d\hat{u}_r/ds$ and $d\hat{h}_r/ds$ are interpolated at this point. In this case we have no v displacement with respect to the central ray (there is however a displacement in time along the central ray) and all the terms in the expansion proportional to v disappear. The program allows an expansion of the electric field which is strictly linear in u_r and h_r (but not v), given directly by eq. (4) and the linearized version of eq. (5). Note that the program allows the last term in eq. (4) to be switched off when an untapered inflector is being run.

The program runs any number of paraxial rays and outputs their optical coordinates as a function of time.

4. EFFECT OF FRINGE FIELD

The analytic electric field calculation discussed in the last section have a hard edge at the beginning and end of the inflector. A real inflector will, of course, have fringe fields, which increase the effective length. This may be observed by running CASINO using a RELAX3D electric potential map, which has been generated from the analytic central ray. Particularly for the case of short inflectors, the effect of these fringe fields may be significant. Fringe fields change the optics of the inflector and push the central ray off the axis of the inflector. This reduces the effective aperture of the inflector, and may lead to a reduced acceptance.

To incorporate the optics of the fringe field into the tracking, and to try to reduce the displacement of the central ray, we have introduced an analytic model for the fringe field into the analytic electric field calculation. In the fringe field model, the electric field is assumed to lie solely in the $\hat{u}_r$ direction. The magnitude of the field is computed using an empirical expression, derived from fitting RELAX3D calculations of the fringe field. A RELAX3D inflector constructed around this analytic central ray shows a consistent effective length. A comparison of the optics for the RELAX3D run and the analytic run with fringe field, shows good agreement.

5. ACCEPTANCE CALCULATION

A separate program calculates the transverse acceptance of the inflector, i.e. the largest volume in the 4-dimensional transverse phase space that passes through the inflector. To illustrate the method of calculation, consider an arbitrary location in the inflector. In the $\hat{u}_r$ direction the aperture is bounded by the electrodes. To prevent the beam being affected by the bad field quality in the fringe field, we assume in our model that the inflector is bounded also in the $\hat{h}_r$ direction by $h_r = \pm a(d/2)$, where d is the plate separation, and a is the aspect ratio. The aspect ratio is the inflector electrode width, divided by the electrode separation. Each of the four boundaries $(\pm u_r, \pm h_r)$ represent a hyper-plane in the phase space which is completely defined if one specifies four points on the plane. The image of the plane at the inflector entrance is found by transforming back these four points, using the inverse of the transfer matrix. The transfer matrices are obtained from running four linearly independent paraxial rays in CASINO. The program divides the inflector into N equidistant sections and at each location transforms back the four hyper-planes. The 4N planes at the entrance then define the acceptance.

To obtain a convenient representation of the acceptance, the program generates a 4-dimensional rectangular mesh of grid points and checks which of these points lie within the acceptance. The distribution of accepted points is then rms-analyzed in order to calculate its second moments and the σ-matrix of the corresponding beam. The phase space volume is proportional to the square root of the σ-matrix determinant.[10]

Due to the transverse coupling in the inflector the calculated acceptance will have correlations between all four phase space variables. In general, such a beam cannot be produced with ordinary optical elements like quadrupoles or solenoids. Therefore, the program also includes the option to calculate the largest uncorrelated beam which can be passed through the inflector. The beam is uncorrelated if the phase space distribution has the property $f(u, p_u, h, p_h) = f(u, p_u, -h, -p_h) = f(-u, -p_u, h, p_h) = f(-u, -p_u, -h, -p_h)$. To find this beam, the program checks not only the grid point (I, J, K, L), but also those points with the above symmetry, to see if they are accepted for given I, J, K, L. If not, the point will be rejected. The uncorrelated acceptance varies with angle between the incoming beam and the electrodes. This angle is an input variable for the program.

6. INFLECTOR ACCEPTANCE RESULTS

Since we wished to study the effect of several inflector parameters on the acceptance, we have chosen to work with the simplest case; namely a constant, homogenous magnetic field. In all cases we have used the hard edge approximation for the entrance into the axial magnetic field at the entrance to the inflector. In addition, to facilitate an analytic exploration of the parameter space we have worked with linear optics.

Figure 1 shows the dependence of acceptance on tilt for an inflector with $A = 2.5$ cm and $R = 1.9$ cm. In all the cases we have studied, the electrodes are tapered. Calculations were done for two representative aspect ratios $a = 1$ and $a = 2$. The calculations included the optics of the analytic model of the fringe field, but for comparison one case is shown where the fringe field is absent. In the $a = 1$ case the acceptance is very flat as a function of k'. While the $a = 2$ case shows a much larger acceptance, which varies with tilt. The correlated acceptance falls to $\sim 50\%$ of the untilted value at $k' = -1.0$ and the uncorrelated acceptance varies by $\sim 40\%$.

Because of the significantly different behaviour for the two values of a, we have examined how the acceptance

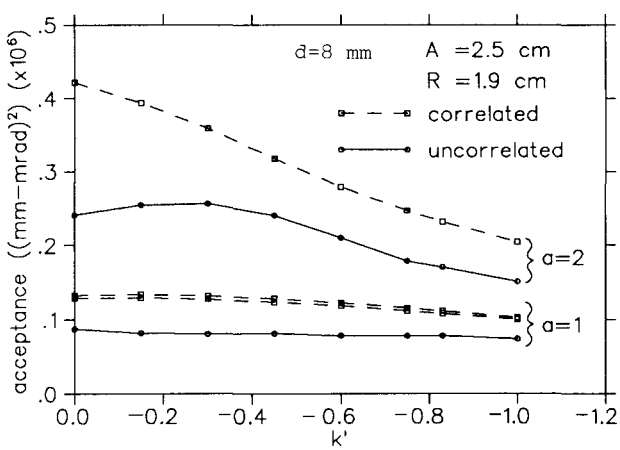

Fig. 1. Acceptance of spiral inflectors as a function of the tilt parameter k'. For comparison the correlated ($a = 1$) case was calculated with fringe field (lower curve) and without (upper curve).

depends on the aspect ratio for inflectors with $k' = 0$ and $k' = -0.83$. The results (see Fig. 2) show that the acceptance increases with a, but then saturates. For the uncorrelated case this happens between $a = 4$ and $a = 8$. This saturation effect may be understood in terms of the coupling present in the inflector. An increase in the aperture of the device in the $\hat{h}_r$ direction (parallel to the electrodes) fails to increase the acceptance after a point, since the particles displaced in this direction couple into the $\hat{u}_r$ direction and hit the electrodes.

We have also investigated several untilted inflectors with different heights (A). In this case (see Fig. 3) we find a very strong decrease in acceptance with increasing height. Once again, the decrease is more pronounced for the case of $a = 2$, and this may be understood again in terms of increased coupling as the inflector becomes taller.

7. SUMMARY

We find that the dependence of the inflector acceptance on tilt is a function of the aspect ratio (a) of the effective aperture in the inflector (as set by poor quality in the fringe field for example). Smaller values of a show less dependence on k'. For a representative case ($a = 2$) we find a strong decrease in the correlated acceptance with tilt, while the uncorrelated acceptance (realizable with common beam line elements) shows a reduced, but significant variation. Finally, the acceptance is found to decrease rapidly with increasing height (A).

One of the reasons for using a tilted inflector is to produce the required orbit centre at the exit of the inflector. It can be shown that in achieving a given orbit centre, one can tradeoff an increase in height, against a decrease in tilt. For the cases studied here, an inflector with $A = 6.6$ cm ($k' = 0$) has the same orbit centre as $A = 2.5$ cm ($k' = -0.83$). In our linear approximation the results show, however, that from the point of view of the acceptance of the inflector, the shorter, tilted inflector is to be preferred. Further work may be required to verify this in the non-linear case.

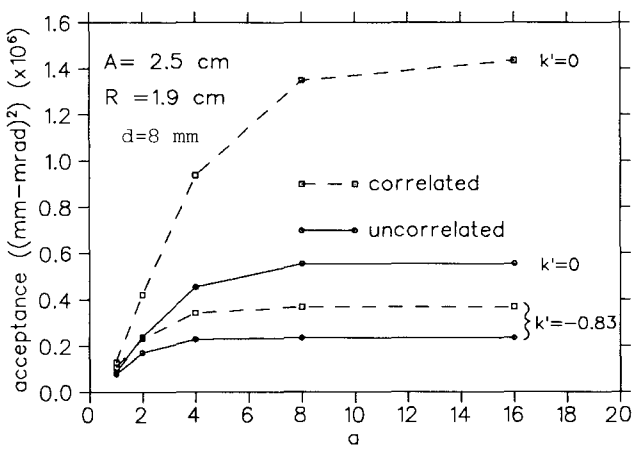

Fig. 2. Acceptance of spiral inflectors as a function of aspect ratio (a).

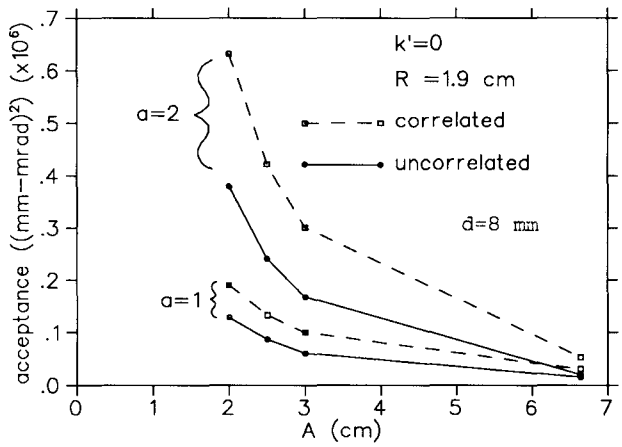

Fig. 3. Acceptance of spiral inflectors as a function of the electric bend radius (A).

REFERENCES

1) Belmont, J.L., Lecture Notes of RCNP Kikuchi Summer School on Accelerator Technology, p. 97, (RCNP, Osaka, 1986).

2) Belmont, J.L. and Pabot, J.L., IEEE Trans. Nucl. Sci., NS-13, 191 (1966).

3) Root, L.W., M.Sc. Thesis, Univ. of British Columbia, Vancouver, 1972.

4) Root, L.W., Ph.D. Thesis, Univ. of British Columbia, Vancouver, 1972.

5) Milton, B.F. and Pearson, J.B., TRIUMF design note TRI-DN-89-19, 1989.

6) Marti, F., Griffin, J. and Taivassalo, V., IEEE Trans. Nucl. Sci., NS-32, 2450, 1985.

7) Balden, R., "Symbolic Mathematical Computation using SMP, Worked Examples 1", TRIUMF design note TRI-DN-89-20, 1989.

8) Kost, C.J. and Jones, F.W., Triumf Internal Report TRI-CD-88-01, 1988.

9) Milinkovic, L., TRIUMF design note TRI-DN-89-21, 1989.

10) Heighway, E.A. and de Jong, M.S., Chalk River Nuclear Laboratories Report, AECL-6975, July 1980, revised June 1984.